Stochastic multi-objective optimisation of the cure process of thick laminates

Tifkitsis, K. I.; Mesogitis, T. S.; Struzziero, G.; Skordos, A. A.

DOI
10.1016/j.compositesa.2018.06.015

Publication date
2018

Document Version
Final published version

Published in
Composites Part A: Applied Science and Manufacturing

Composites Part A 112 (2018) 383–394

Contents lists available at ScienceDirect

Composites Part A

journal homepage: www.elsevier.com/locate/compositesa

Stochastic multi-objective optimisation of the cure process of thick laminates

K.I. Tifkitsis[a,*], T.S. Mesogitis[b], G. Struzziero[c], A.A. Skordos[a]

[a] School of Aerospace, Transport and Manufacturing, Cranfield University, Bedford MK43 0AL, UK
[b] National Composites Centre, Bristol BS16 7FS, UK
[c] Faculty of Aerospace, Structural Integrity & Composites, Delft University of Technology, Delft 2628 CD, Netherlands

ARTICLE INFO

Keywords:
A. Carbon fibre
A. Thermosetting resin
C. Process simulation
E. Cure

ABSTRACT

A stochastic multi-objective cure optimisation methodology is developed in this work and applied to the case of thick epoxy/carbon fibre laminates. The methodology takes into account the uncertainty in process parameters and boundary conditions and minimises the mean values and standard deviations of cure time and temperature overshoot. Kriging is utilised to construct a surrogate model of the cure substituting Finite Element (FE) simulation for computational efficiency reasons. The surrogate model is coupled with Monte Carlo and integrated into a stochastic multi-objective optimisation framework based on Genetic Algorithms. The results show a significant reduction of about 40% in temperature overshoot and cure time compared to standard cure profiles. This reduction is accompanied by a reduction in variability by about 20% for both objectives. This highlights the opportunity of replacing conventional cure schedules with optimised profiles achieving significant improvement in both process efficiency and robustness.

1. Introduction

The optimisation of the manufacturing of continuous fibre thermosetting matrix composites is critical for minimising cost and the likelihood of occurrence of process failures defects. During the process of cure, the thermosetting resin transforms from an oligomeric liquid to a glassy solid through an exothermic crosslinking reaction. In the case of thick components the heat generated due to the reaction can lead to severe temperature overshoots. These can affect considerably the quality of the manufactured component. The risks associated with temperature overshoots in thick components are dealt with by adopting conservative cure cycles. This in turn results in long processing times and high manufacturing costs.

The selection of optimal cure profiles that can minimise cure time and the occurrence of temperature overshoots or other process-induced defects has been addressed in the literature using single-objective and multi-objective optimisation. Cure time can be reduced by up to 30% for thick parts [1–3] and 50% for ultra-thick parts [4–6], whereas targeting the minimisation of residual stresses in a single-objective profile optimisation context can lead to their reduction by about 30% [7–12]. The optimal solutions obtained in single optimisation setups merging objectives in a weighted sum [13,14] are dependent on the weights which imply a relative prioritisation between the different objectives. Multi-objective optimisation can overcome this limitation by treating the two objectives independently. An approach of this type based on Genetic Algorithms (GAs) has been used to address cure time and temperature overshoot minimisation in thick parts [15]. The results have shown the existence of a trade-off between the two objectives with an L shaped Pareto front incorporating solutions that can achieve improvements of about 50% with respect to both cure time and overshoot compared to standard cure profiles. However, the benefits offered by the exploration of the design space by numerical optimisation can be accompanied by relative instability of some of the solutions with respect to perturbations of nominal process parameters leading to potential risks.

The process of cure involves several sources of variability including environmental/boundary conditions uncertainty and material properties variations [16]. Stochastic simulation has shown that amongst these, tool temperature has the greatest impact on cure time variability [17]. Uncertainty in preform architecture, such as fibre misalignment, can cause variability in residual stresses and also in final distortion of the cured part [18]. Variability in cure kinetics parameters, such as initial degree of cure, activation energy and reaction order, can induce significant variations in temperature overshoot reaching coefficients of variation of approximately 30% [19]. Uncertainty in surface heat transfer and tool temperature can cause significant variability in cure

* Corresponding author.
E-mail address: k.tifkitsis@cranfield.ac.uk (K.I. Tifkitsis).

https://doi.org/10.1016/j.compositesa.2018.06.015
Received 13 April 2018; Received in revised form 6 June 2018; Accepted 9 June 2018
Available online 11 June 2018

time reaching a coefficient of variation of 20% [20]. In the case of optimisation, the level of uncertainty in boundary conditions affects significantly the optimal solution [21]. Consideration of the effects of variability and the potential lack of stability of optimised solutions suggest that the combination of multi-objective optimisation with stochastic simulation is relevant for cure process design aiming to address simultaneously efficiency and robustness.

The present paper describes the development of a methodology for the incorporation of variability in multi-objective optimisation of composites cure. The variability in boundary conditions during curing is characterised and represented using appropriate stochastic objects. An existing multi-objective optimisation methodology of the cure based on GAs [15] is integrated with Monte Carlo to incorporate variability of cure time and temperature overshoot in the set of objectives considered. A surrogate model of the cure is developed using the Kriging method substituting the FE model in the Monte Carlo simulation to reduce the computation effort required for the combination of optimisation and stochastic simulation. The methodology is applied to the cure of a thick flat carbon fibre/epoxy laminate.

2. Methodology

2.1. Cure simulation

A heat transfer cure simulation model was implemented in the Finite Element (FE) solver MSC. Marc to represent the cure of a Hexcel G1157 pseudo unidirectional carbon fibre/Hexcel RTM6 epoxy resin flat panel. The model comprises 26 3-D 8 noded iso-parametric composite brick elements (MSC. Marc element type 175 [22]) representing a 15.6 mm thick laminate. Although the dimensionality of the solution is 3-D, the heat transfer problem is one-dimensional requiring the use of only one element across the in-plane dimensions. Each element represents two layers of fabric with a thickness of 0.3 mm each.

Fig. 1 illustrates a schematic representation of the model. The boundary conditions were implemented using user subroutines FORCDT and UFILM for time dependent prescribed temperature and forced air convection respectively [23]. User subroutines UCURE, USPCHT, and ANKOND were used for cure kinetics, specific heat capacity and thermal conductivity material sub-models [23].

The cure kinetics model for the resin system of this study is a combination of an n^{th} order term and an autocatalytic term [24]:

$$\frac{d\alpha}{dt} = k_1(1-\alpha)^{n_1} + k_2(1-\alpha)^{n_2}\alpha^m \quad (1)$$

where α is the instantaneous degree of cure, m, n_1, n_2 the reaction orders and k_1 and k_2 the reaction rate constants defined as follows:

$$\frac{1}{k_i} = \frac{1}{k_{i,C}} + \frac{1}{k_d},\ i = 1, 2 \quad (2)$$

Here $k_{i,C}$ are Arrhenius functions of temperature for the chemical reaction and k_d is a diffusion rate constant, which expresses the deceleration of the reaction as the instantaneous glass transition of the curing material approaches the cure temperature. These are expressed as follows:

$$k_{i,C} = A_d e^{(-E_i/RT)},\ i = 1, 2 \quad (3)$$

$$k_d = A_i e^{(-E_d/RT)} e^{(-b/f)} \quad (4)$$

where A_i, A_d are pre-exponential factors, b is a fitting parameter, E_i and E_d the activation energy for the chemical reactions and diffusion respectively, T is the absolute temperature, R the universal gas constant and f the equilibrium free volume, which is expressed as follows:

$$f = w(T-T_g) + g \quad (5)$$

Here w and g are constants and T_g is the instantaneous glass transition temperature following the Di Benedetto equation [25]:

$$T_g = T_{g0} + \frac{(T_{g\infty}-T_{g0})\lambda\alpha}{1-(1-\lambda)\alpha} \quad (6)$$

where $T_{g\infty}$ and T_{g0} are the glass transition temperature of the fully cured and uncured material and λ is a parameter controlling the convexity of the dependence. Model constants are reported in Table 1 [19].

The specific heat capacity of the composite is computed making use of the rule of mixtures as follows:

$$c_p = w_f c_{pf} + (1-w_f)c_{pr} \quad (7)$$

where w_f is the fibre weight fraction, c_{pf} the fibre specific heat capacity and c_{pr} the specific heat capacity of the resin. The specific heat capacity

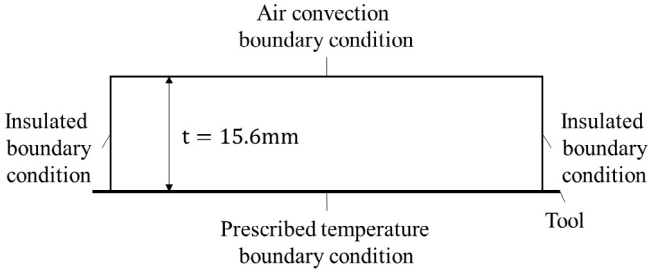

Fig. 1. Schematic representation of the cure model.

Table 1
Parameters values for the cure kinetics [19], glass transition temperature, specific heat capacity [15], thermal conductivity [1] and density material models [27,28].

Parameter		Value
Pre-exponential factor of the nth order term	A_1	19,000 (s^{-1})
Pre-exponential factor of the autocatalytic term	A_2	22,080 (s^{-1})
Pre-exponential factor of diffusion	A_d	6.7610^{18} (s^{-1})
Activation energy of the nth order term	E_1	72,900 ($Jmol^{-1}$)
Activation energy of the autocatalytic term	E_2	57,820 ($Jmol^{-1}$)
Activation energy of diffusion	E_d	138,000 ($Jmol^{-1}$)
Autocatalytic reaction order	m	1.29
Reaction order of the nth order term	n_1	1.97
Reaction order of the autocatalytic term	n_2	1.53
Exponent of diffusion term	b	0.452
Equilibrium free volume model slope	w	0.00048 (1/K)
Equilibrium free volume model intercept	g	0.025
Glass transition temperature of uncured material	T_{g0}	−11 (°C)
Glass transition temperature of fully cured material	$T_{g\infty}$	206 (°C)
Glass transition temperature convexity constant	λ	0.435 ($Jg^{-1}°C^{-2}$)
Fibre specific heat capacity model slope	A_{fc_p}	0.0023 ($Jg^{-1}°C^{-2}$)
Fibre specific heat capacity model intercept	B_{fc_p}	0.765 ($Jg^{-1}°C^{-2}$)
Resin specific heat capacity model slope	A_{rc_p}	0.0025 ($Jg^{-1}°C^{-2}$)
Resin specific heat capacity model intercept	B_{rc_p}	1.8 ($Jg^{-1}°C^{-2}$)
Resin specific heat capacity model step	Δ_{rc_p}	−0.25 ($Jg^{-1}°C^{-2}$)
Resin specific heat capacity model step breadth parameter	C_{rc_p}	1.1 ($°C^{-1}$)
Resin specific heat capacity model step shift parameter	σ	16.5 (°C)
Fibre transverse thermal conductivity	B_{tf}	0.84 ($Wm^{-1}°C^{-2}$)
Resin thermal conductivity model quadratic coupling	a_{Kr}	0.0008 ($Wm^{-1}°C^{-2}$)
Resin thermal conductivity model coupling constant	b_{Kr},	−0.0011 ($Wm^{-1}°C^{-2}$)
Resin thermal conductivity model linear temperature constant	c_{Kr},	−0.0002 ($Wm^{-1}°C^{-2}$)
Resin thermal conductivity model quadratic conversion constant	d_{Kr},	−0.0937 ($Wm^{-1}°C^{-2}$)
Resin thermal conductivity model linear conversion constant	e_{Kr},	0.22 ($Wm^{-1}°C^{-2}$)
Resin thermal conductivity model intercept	f_{Kr}	0.12 ($Wm^{-1}°C^{-2}$)
Resin density	ρ_r	1.11 (gml^{-1})
Fibre density	ρ_f	1.76 (gml^{-1})

of the resin and the fibre are computed using the models [15]:

$$c_{pf} = A_{fc_p}T + B_{fc_p} \tag{8}$$

$$c_{pr} = A_{rc_p}T + B_{rcp} + \frac{\Delta_{rc_p}}{1 + e^{C_{rc_p}(T-T_g-\sigma)}} \tag{9}$$

where A_{fc_p}, B_{fc_p} control the linear dependence of fibre specific heat capacity on temperature, A_{rc_p}, B_{rc_p} describe the linear dependence of the specific heat capacity of the uncured epoxy on temperature and Δ_{rc_p}, C_{rc_p}, and σ are the strength, width and temperature shift of the specific heat capacity step occurring at resin vitrification. The values of the parameters involved in Eqs. (8)-(9) are reported in Table 1 [15].

The thermal conductivity of the composite in the through thickness direction is computed using a geometry-based model [26] as follows:

$$K_{22} = K_{33} = v_f K_r\left(\frac{K_{tf}}{K_r}-1\right) + K_r\left(\frac{1}{2}-\frac{K_{tf}}{2K_r}\right) + K_r\left(\frac{K_{tf}}{K_r}1\right)\sqrt{v_f{}^2 - v_f + \frac{\left(\frac{K_{tf}}{K_r}+1\right)^2}{\left(\frac{2K_{tf}}{K_r}-2\right)^2}} \tag{10}$$

where K_{tf} is the thermal conductivity of the fibre in the transverse direction. The thermal conductivity of the carbon fibre in the transverse direction can be expressed as follows:

$$K_{tf} = B_{tf} \tag{11}$$

where B_{tf} is a constant. The thermal conductivity for the epoxy resin system RTM6 is a function of degree of cure and temperature and is expressed as [1]:

$$K_r = a_{Kr}T\alpha^2 + b_{Kr}T\alpha + c_{Kr}T + d_{Kr}\alpha^2 + e_{Kr}\alpha + f_{Kr} \tag{12}$$

Here a_{Kr}, b_{Kr}, c_{Kr}, d_{Kr}, e_{Kr}, f_{Kr} are coefficients of the polynomial function. The parameters of the thermal conductivity model are reported in Table 1 [1].

The density of the composite can be calculated using the density of the constituents:

$$\rho = \frac{\rho_c\rho_f}{w_f\rho_r + (1-w_f)\rho_f} \tag{13}$$

where ρ_r and ρ_f are the densities of resin and fibres respectively and are reported in Table 1 [27,28].

2.2. Surrogate model

Cure simulation using FE analysis is computationally expensive. When stochastic simulation using Monte Carlo and multi-objective optimisation based on GAs are combined, the number of function evaluations of the FE model becomes too large to handle with conventional computing resources. A surrogate model was developed using the Kriging method to overcome this issue by substituting the FE solution. Kriging allows the unbiased estimation of untried parameter values to be made with minimum variance and more accurately in comparison with low order polynomial regression [29]. Fig. 2 illustrates the procedure of surrogate model development adopted in this work. Kriging requires a set of sampling points at which the model response is known. Latin Hypercube Sampling [30] was utilised for generating a large sample of M points in this work, whilst the FE model of the cure was used to compute the response at these points. Taking into account the dimensionality and the nonlinear character of the problem and following preliminary testing of the behaviour of the surrogate model, a sample of 30,000 points was selected.

The input variables of the surrogate model include the optimisation parameters and the variables that have significant variability and are considered stochastic. These are parameters of the two-dwell cure profile illustrated in Fig. 3, such as the temperature of first (T_1) and second dwell (T_2), the duration of the first dwell (dt_1) and the heat ramp rate (r) and stochastic process variables such as the surface heat transfer coefficient (h), the activation energy (E_2) and reaction order (m) of the autocatalytic component of the cure kinetics model and the initial degree of cure (α_0). The surrogate modelling methodology treats these in the same way, with some of them such as dwell temperature having a dual role both as optimisation parameters and stochastic variables. Table 2 summarises the role and ranges of parameters and variables considered in the surrogate model. The cure kinetics parameter ranges reported in Table 2 were set taking into account their average and standard deviation as quantified in a previous study [19]. The outputs of the surrogate model, which correspond to the two variables considered in the optimisation, are the cure time (t_{cure}) and the maximum temperature overshoot (ΔT_{max}). Cure time is defined as the time at which the minimum degree of cure of the part is greater than 88%, which is the degree of cure that RTM6 reaches during an isothermal Differential Scanning Calorimetry test at 180 °C [31]. When the degree of cure reaches this threshold the simulation ends. Consequently, the second dwell time is not a design parameter in the optimisation. The temperature overshoot is defined as the maximum difference between the tool control temperature and the temperature in the composite during the process.

The Kriging metamodel expresses the model response $Y(\mathbf{x}) \in \mathbb{R}$ (cure time or maximum temperature overshoot) for the input vector $\mathbf{x} = [T_1, T_2, dt_1, r, h, E_2, m, \alpha_0]$, $\mathbf{x} \in \mathbb{R}^8$as follows:

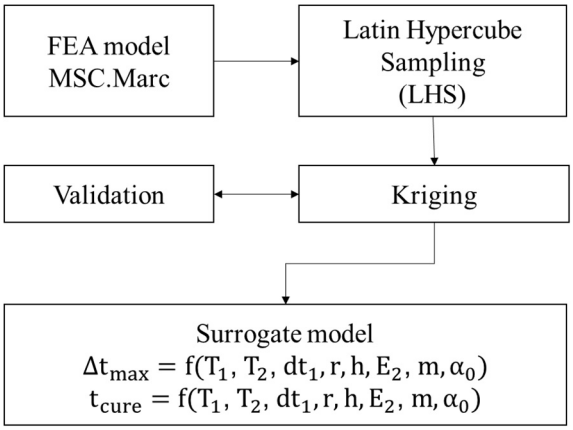

Fig. 2. Surrogate model construction methodology.

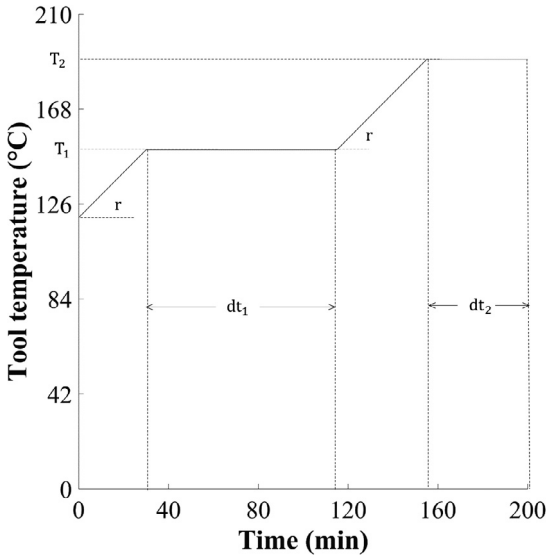

Fig. 3. Two-dwell cure profile.

Table 2
Range and role of surrogate model input parameters.

Parameter		Range	Optimisation variable	Stochastic variable
First dwell temperature	T_1 (°C)	135–175	Yes	Yes
Second dwell temperature	T_2 (°C)	175–215	Yes	Yes
Duration of first dwell	dt_1 (min)	33–300	Yes	No
Heating rate	r (°C/min)	1–4	Yes	No
Surface heat transfer coefficient	h ($W/m^2/°C$)	13.8–21.8	No	Yes
Autocatalytic activation energy	E_2 (KJ/mol)	56–59.6	No	Yes
Autocatalytic reaction order	m	1–1.6	No	Yes
Initial degree of cure	α_0 (%)	1.5–5.1	No	Yes

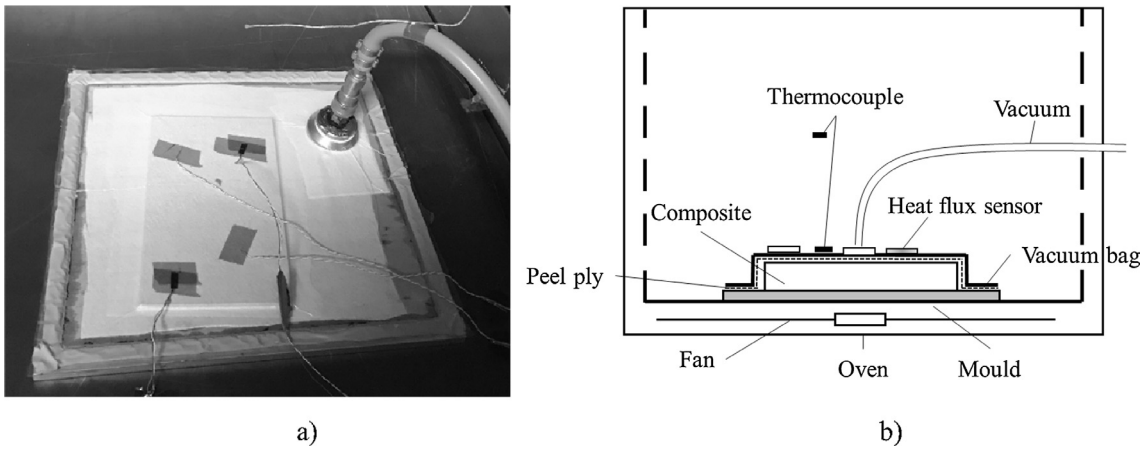

Fig. 4. (a) Infusion set up with the sensors (b) Schematic representation of experimental set-up.

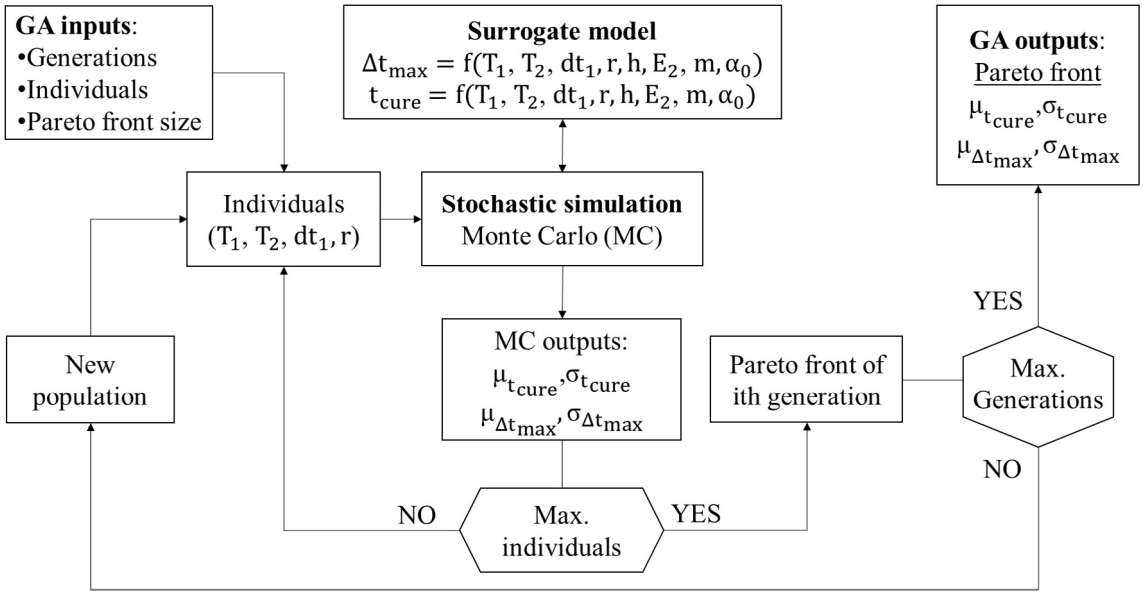

Fig. 5. Stochastic multi-objective optimisation methodology.

Table 3
GA parameters used for stochastic optimisation.

GA input	Value
Max Number of generations	12
Individuals per population	70
Individuals per reproduction	50
Elite individuals	6
Size of Pareto set	40
Mutation probability	0.005
Cross-over probability	0.5

$$Y(\mathbf{x}) = \mathbf{f}(\mathbf{x})^T\boldsymbol{\beta} + \mathbf{r}(\mathbf{x})^T\boldsymbol{\gamma}^* \quad (14)$$

where the term $\mathbf{f}(\mathbf{x})^T\boldsymbol{\beta}$ corresponds to a 2nd order regression model expressing the output variable (t_{cure} or ΔT_{max}) as a linear combination of p basis functions $f_i(\mathbf{x})$: $\mathbb{R}^p \mapsto \mathbb{R}$ expressed as:

$$\mathbf{f}(\mathbf{x})^T\boldsymbol{\beta} = \beta_1 f_1(\mathbf{x}) + \cdots + \beta_p f_p(\mathbf{x}) \quad (15)$$

Here $\boldsymbol{\beta} \in \mathbb{R}^p$ is the vector of regression parameters computed using generalised least squares and p is:

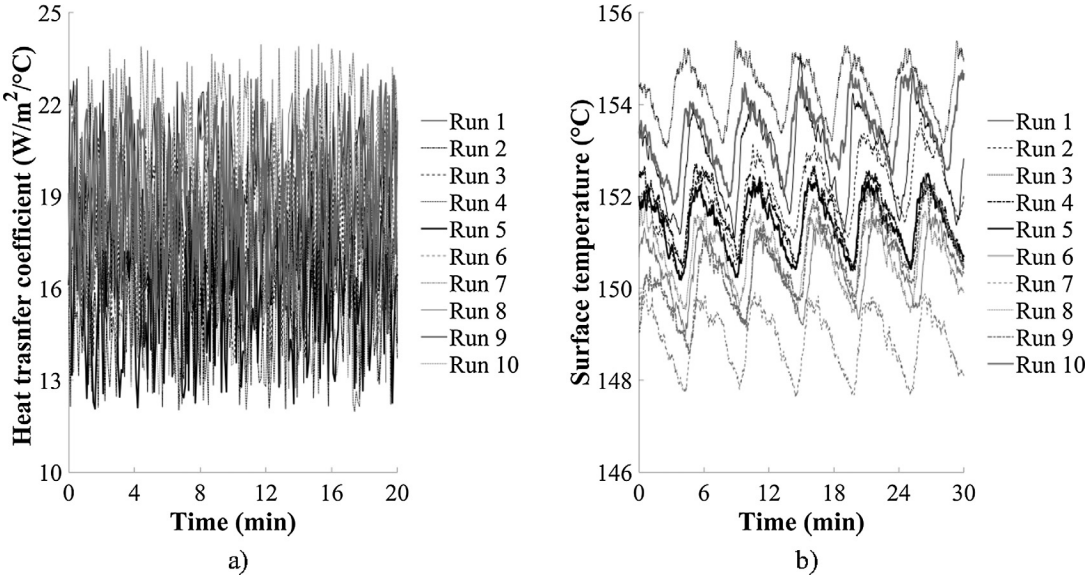

Fig. 6. Experimental results of (a) heat transfer coefficient (b) surface temperature.

Table 4
Stochastic properties of cure kinetics parameters [19] and boundary conditions.

	α_0	m	E_2 (J/mol)	h (W/m²/°C)	T_s (°C)
Average	0.033	1.29	57, 820	17.8	151.8
Standard deviation	0.006	0.094	600	1.3	1.6

$$p = \frac{(n+1)(n+2)}{2} \tag{16}$$

with n the dimensionality of the model, which is 8 in the case considered here.

The term $\mathbf{r}(\mathbf{x})$ corresponds to a vector of cross-correlations between input point $\mathbf{x}$ and each of M sampling points ($\mathbf{s_x} \in \mathbb{R}^8$):

$$\mathbf{r}(\mathbf{x}) = [R(\theta, \mathbf{x}, \mathbf{s_x^1}), \cdots, R(\theta, \mathbf{x}, \mathbf{s_x^M})]^T \tag{17}$$

Here $R(\theta, \mathbf{x}, \mathbf{s_x^k})$ denotes the correlation between input point $\mathbf{x}$ and sampling point $\mathbf{s_x^k}$ and depends on the parameter vector $\theta \in \mathbb{R}^8$ and the distance between them. A Gaussian function was chosen for the correlation structure as follows:

$$R(\theta, \mathbf{x}, \mathbf{s}) = e^{-\theta_k d_k^2}, \; d_k = x_k - s_k, \; k = 1, \cdots, 8 \tag{18}$$

The parameter vector θ allows the correlation function to represent anisotropy in the correlation across different directions of the model. The optimal correlation parameter vector θ can be estimated by solving the following optimisation problem [32]:

$$\theta = \mathbf{argmin}\left(|\mathcal{R}|^{\frac{1}{M}}\sigma^2\right) \tag{19}$$

where $|\mathcal{R}|$ is the determinant of the correlation matrix $\mathcal{R} \in \mathbb{R}^{M\times M}$ of all sampling points involved in the model and σ^2 is the predictor Gaussian process variance, expressed as follows [33]:

$$\sigma^2 = \frac{1}{M}[s_y^1 - \mathbf{f}(\mathbf{s_x^1})^T\boldsymbol{\beta} \cdots s_y^M - \mathbf{f}(\mathbf{s_x^M})^T\boldsymbol{\beta}]\mathcal{R}^{-1}\begin{bmatrix} s_y^1 - \mathbf{f}(\mathbf{s_x^1})^T\boldsymbol{\beta} \\ \vdots \\ s_y^M - \mathbf{f}(\mathbf{s_x^M})^T\boldsymbol{\beta} \end{bmatrix} \tag{20}$$

The optimisation problem in Eq. (19) is combined with the estimation of the regression coefficients ($\boldsymbol{\beta}$) in Eq. (15) and of the process variance (σ^2) based on maximising the likelihood of responses $s_y^1, \ldots, s_y^M$ at sampling points $\mathbf{s_x^1}, \ldots, \mathbf{s_x^M}$ respectively.

Vector $\boldsymbol{\gamma}^* \in \mathbb{R}^M$ is computed as follows:

$$\boldsymbol{\gamma}^* = \mathcal{R}^{-1}\begin{bmatrix} s_y^1 - \mathbf{f}(\mathbf{s_x^1})^T\boldsymbol{\beta} \\ \vdots \\ s_y^M - \mathbf{f}(\mathbf{s_x^M})^T\boldsymbol{\beta} \end{bmatrix} \tag{21}$$

The estimation problem corresponding to Eqs. (14)-(21) was implemented and solved using the MATLAB® toolbox for Kriging modelling [34]. The resulting predictor (Eq. (14)) was implemented in Visual Studio C++.

2.3. Stochastic simulation

2.3.1. Quantification of boundary conditions variability

Boundary conditions variability has been quantified in a series of 10 experiments carried out utilising the setup depicted in Fig. 4. The setup includes a Caltherm E9321V2 oven with an Eurotherm 2408P4 PID controller, a 10 mm aluminium tool plate, nylon N64PS-x VAC Innovation peel ply fabric, nylon xR1.2 VAC Innovation vacuum bag, three K-type thermocouples and two RdF micro-foil heat flux sensors [35]. A 5 mm composite flat panel was used to create thermal conditions similar to those during the cure of a composite part. The matrix system of the panel was Hexcel RTM6 and the reinforcement Hexcel G1157 pseudo unidirectional carbon fabric with an areal density of 277 g/m². The composite part was placed on the tooling plate, covered with the peel ply and the vacuum bag and sealed before the experimental runs.

Table 5
Input parameters values used for the construction of the response surfaces of the two validation test cases.

	T_1 (°C)	T_2 (°C)	dt_1 (min)	r (°C/min)	h (W/m²/°C)	E_2 (J/mol)	m	α_0
1st Case	135–175	175–215	84	2	17.8	57820	1.29	0.033
2nd Case	135–175	195	84	1–4	17.8	57820	1.29	0.033

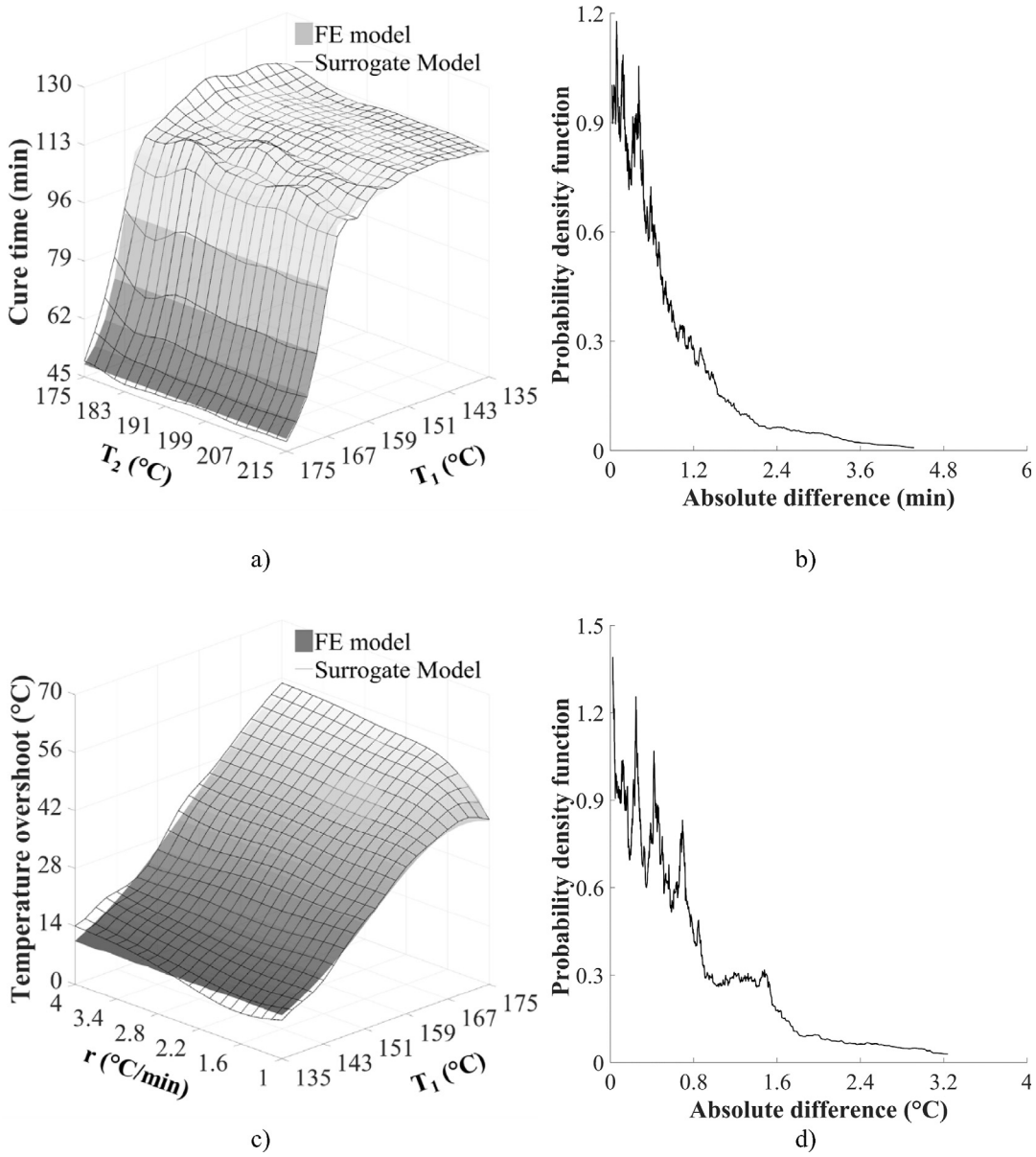

Fig. 7. FE and surrogate model response surfaces: (a) Case 1 (Table 5) cure time as a function of the first and second dwell temperature; (b) PDF of absolute differences between surrogate and FE model for Case 1 (c) Case 2 (Table 5) temperature overshoot as a function of first dwell temperature and ramp; (d) PDF of absolute differences between surrogate and FE model for Case 2.

Two K-type thermocouples were mounted on the bag to monitor the surface temperature, whilst the third one was placed outside the thermal boundary layer and close to the surface to measure air temperature. Two heat flux sensors were placed on the vacuum bag to measure the convection heat flux and its variability. The micro-foil flux sensor outputs a voltage signal which is proportional to the heat flux with the proportionality coefficient determined individually per sensor by the supplier [35]. The heat transfer coefficient is calculated using the temperatures of the surface (T_s) and air in the oven (T_{air}) and the measured heat flux ($\dot{Q}$) as follows:

$$h = \frac{\dot{Q}}{T_s - T_{air}} \tag{22}$$

The temperature was set up at 160 °C during all runs. A National Instruments LabVIEW in-house code was used for data acquisition and the data were acquired with a frequency of 0.8 Hz for 20 min and 30 min after the oven temperature controller reached a plateau at 160 °C for the heat transfer coefficient and surface temperature measurements respectively.

2.3.2. Monte Carlo simulation

The stochastic simulation is based on Monte Carlo (MC). The implementation carried out in Visual Studio C++ involves the generation of N_{MC} realisations of random input stochastic variables using the Mersenne Twister random number generator [36]. The MC sampling points are generated using an orthogonal set of normally distributed uncorrelated random variables. The transformation from the stochastic variables of the problem to the set of uncorrelated random variables is carried out using Cholesky decomposition. In the particular setup addressed in this work there two pairs of correlated variables. These are the autocatalytic reaction order (m) and the initial degree of cure (α_0) with a correlation coefficient of 0.55 and the autocatalytic activation energy (E_2) and reaction order (m) with a correlation coefficient of −0.84 [19]. In each realisation, the surrogate model is executed calculating the process outcomes (cure time and temperature overshoot) and subsequently computing their first and second statistical moments

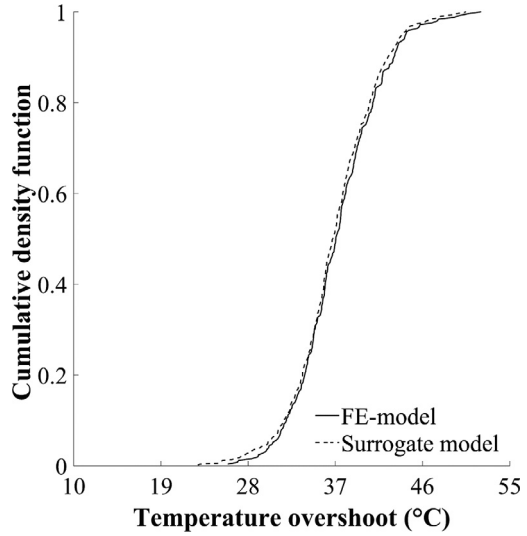

Fig. 8. Cumulative density function (CDF) of a standard cure profile of temperature overshoot.

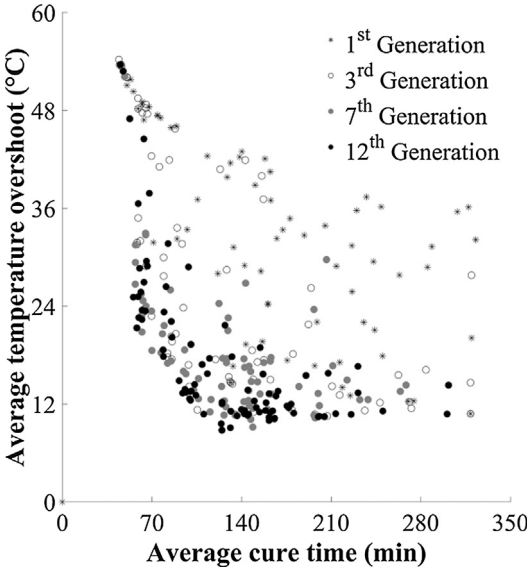

Fig. 9. Population evolution of stochastic multi-objective optimisation.

using the overall set of realisations. A total of 500 realisations is required to ensure convergence in average and standard deviation. The outputs of the stochastic simulation are the average and standard deviation of cure time and of temperature overshoot.

2.4. Stochastic multi-objective optimisation

The aim of stochastic multi-objective optimisation is to minimise cure time, temperature overshoot and their variability. These are captured by a set of four minimisation objectives, i.e. the means and standard deviations of the two metrics. The ranges of potential values for each design variable are summarised in Table 2. The stochastic simulation was integrated with a GA for multi-objective optimisation [15] by developing an appropriate interface. The stochastic optimisation framework illustrated in Fig. 5 was implemented in Visual Studio C++. The parameters of the GA are reported in Table 3. The output of the GA is the Pareto set of optimal design parameters and the corresponding objective values.

3. Results and discussion

3.1. Stochastic objects

Fig. 6a and 6b illustrate the results of heat transfer coefficient and surface temperature evolution variability experiments. Both parameters present two types of variations: (i) variations over time (short term variability), and (ii) level variability across the different experiments. The air streams inside the oven produced by its fan cause forced convection and short term variability in heat transfer coefficient and surface temperature. The forced convection results in higher values of heat transfer coefficient in comparison with natural convection which is in the range of 10–15 $W/m^2/°C$ [20]. The level variability across different experimental runs of both heat transfer coefficient and surface temperature can be attributed to the varying laboratory conditions. The surface temperature includes also a periodic term representing a dependence on time, which can be attributed to temperature control in the oven. The corresponding periodic fluctuation is in the range of 2 °C around the set temperature.

Stochastic objects for the heat transfer coefficient and surface temperature are utilised to incorporate the corresponding variability into the stochastic simulation scheme. Short term variability of heat transfer coefficient and tool temperature has negligible influence on the process outcomes and only the variability of the level needs to be taken into account [20]. Therefore the surface heat transfer coefficient and the surface temperature are modelled using random series of observations as follows:

$$T_s = \mu_s + \sigma_s y_T \quad (23)$$

$$h = \mu_h + \sigma_h y_h \quad (24)$$

where y_T and y_h denote independent identically distributed standard normal variables, μ_s and μ_h the mean values and σ_s, σ_h the standard deviations of heat transfer coefficient and surface temperature respectively. The average values and the corresponding standard deviations are reported in Table 4.

3.2. Surrogate model validation

Response surfaces, representing the relationship between process outputs and inputs, for two different cases detailed in Table 5 were constructed to assess the accuracy of the surrogate model. The response surface of t_{cure} over the space of T_1 and T_2 is illustrated in Fig. 7a for constant values for the rest of the input parameters (dt_1, r, h, m, E_2, α_0) as reported in Table 5 (Case 1). It can be observed that, for the particular values of parameters considered, increasing T_1 reduces cure time significantly, whilst the effect of T_2 is weaker. The reduction of cure time is non-linear with increasing temperature as a consequence of the non-linear nature of cure. The negligible influence of the second dwell temperature on cure time in the region of high first dwell temperatures is attributed to the fact that the cure process is already completed before the second dwell. The contribution of T_2 is of importance when the first dwell temperature is below 165 °C, in which case the cure time is decreasing with increasing T_2. The comparison of the two surfaces illustrated in Fig. 7a shows that the surrogate model is an accurate representation of the FE cure simulation. The mean absolute difference between the two is 0.9 min, which represents a very small percentage of cure time (0.5% to 2%). Fig. 7b illustrates the probability density function (PDF) of absolute difference between the FE and surrogate models. The region with the highest probability is between 0 and 0.7 min, with probability becoming very small over 1.2 min.

Fig. 7c illustrates the dependence of ΔT_{max} on T_1 and r for constant values for the rest of the parameters (T_2, dt_1, h, m, E_2, α_0) as reported in Table 5 (Case 2). The agreement between the surrogate model and the simulation is very good. The temperature overshoot increases with increasing T_1. In the region of low heating ramp and high first dwell

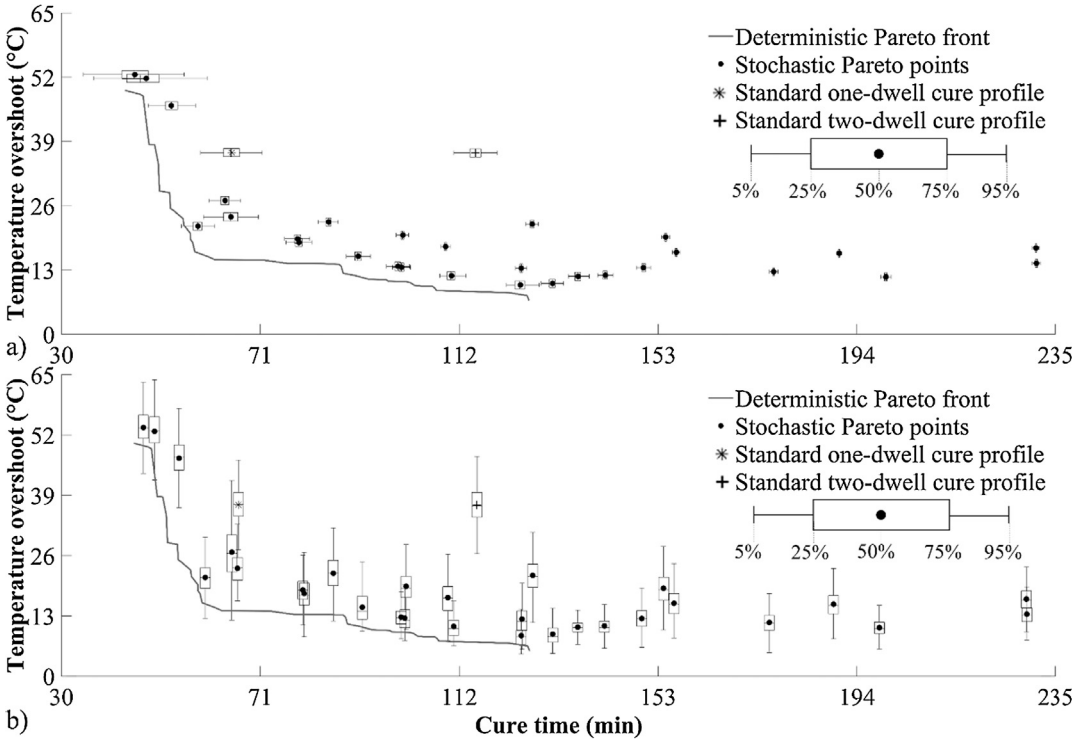

Fig. 10. Pareto front of stochastic and deterministic multi-objective optimisation (a) cure time box plots; (b) temperature overshoot box plots.

Table 6
Sensitivity analysis of deterministic and stochastic optimal points.

	Stochastic optimal point	Deterministic optimal point
1st dwell temperature (°C)	144	152
2nd dwell temperature (°C)	214	214
Dwell duration (min)	35	33
Heating ramp (°C/min)	3.7	3.8
Average cure time (min)	58	55
Average temperature overshoot (°C)	21	27
Cure time standard deviation (min)	1.3	1.9
Temperature overshoot standard deviation (°C)	3.6	6.6

temperature, the temperature overshoot decreases with increasing first dwell temperature as a result of the occurrence of maximum reaction during the ramp. The PDF of absolute error (Fig. 7d) indicates that the region of high probability is between 0 and 0.8 °C. The mean absolute error is 0.9 °C, whilst the probability of error greater than 1.6 °C is negligible.

The surrogate model accuracy was also tested in the case of MC simulation. A standard two dwell cure profile with first dwell temperature of 160 °C for 75 min and second dwell temperature of 180 °C [28] was simulated using 500 realisations. Fig. 8 illustrates the cumulative density function (CDF) of temperature overshoot as computed by the FE and surrogate models. The average temperature overshoot is 37 °C, whilst the standard deviation is 4.5 °C implying a coefficient of variation equal to 12%. It can be observed that the two CDFs are in very close agreement. The computational time of stochastic simulation is reduced significantly with the use of the surrogate model. The stochastic simulation using FE takes 420 min on a Quad Core CPU (3.6 GHz) PC, whilst the surrogate model based solution needs 3 min. This represents a reduction by more than 99%.

3.3. Stochastic multi-objective optimisation

The evolution of the GA population during stochastic multi-objective optimisation run is illustrated in Fig. 9 in terms of mean cure time and temperature overshoot. As the stochastic optimisation progresses, the population sample is improved compared to populations of previous generations. The GA converges – i.e. the Pareto set is stabilised – between 7 and 12 generations. Fig. 10 shows the average cure time-average temperature overshoot cross section of the stochastic Pareto front, with the variability with respect to both variables in box plots. The deterministic Pareto front is also illustrated with a solid line. The Pareto fronts of both the stochastic and deterministic optimisation are in the form of an L-shape curve comprising two regions: (i) a horizontal region in which cure time can be reduced significantly without considerable changes in temperature overshoot; and (ii) a vertical region in which high temperature overshoots occur with small changes in cure time. The majority of the stochastic Pareto points are shifted up compared to the deterministic Pareto front. The stochastic Pareto set includes points in which the mean values are dominated by other optimal points, but they dominate them in terms of variability resulting in a 4-D front. In contrast, in the deterministic case the domination ranking occurs only in terms of nominal values and consequently the Pareto front is 2-D.

Deterministic optimisation finds the solutions minimising the objectives without considering the variation of the solution potentially yielding optimal points with high sensitivity to variability. This can be problematic, especially in cases where the deterministic optimisation exploits high sensitivity areas of the landscape. For example, optimal points in the vertical region of the deterministic Pareto set can be highly sensitive to variations resulting in temperature overshoots significantly different than predicted by the simulation. This possibility necessitates the use of more conservative cure profiles. In order to demonstrate this weakness of deterministic optimisation and the way the stochastic optimisation can overcome it, two points of the vertical region of deterministic and stochastic Pareto front with similar cure time and temperature overshoot were selected and analysed. The details of these

Table 7
Comparison of optimal and standard cure profiles and their response under aggressive and conservative uncertainty scenarios.

		Short dwell optimal profile	Intermediate dwell optimal profile	Standard one dwell profile	Standard two dwell profile
Cure profile	T_1 (°C)	147	139	180	160
	T_2 (°C)	189	209	–	180
	dt_1 (min)	38	56	120	75
	r (°C/min)	3	2	1	1.5
Mean realisation	T_1 (°C)	147	139	180	160
	T_2 (°C)	189	209	–	180
	h (W/m^2/°C)	17.8	17.8	17.8	17.8
	E_2 (J/mol)	57,820	57,820	57,820	57,820
	m	1.29	1.29	1.29	1.29
	α_0	0.033	0.033	0.033	0.033
	Cure time (min)	65	90.6	66	115
	Overshoot (°C)	22	12	37.3	37
Aggressive realisation	T_1 (°C)	150	142	183	163
	T_2 (°C)	192	212	–	183
	h (W/m^2/°C)	15.1	15.1	15.1	15.1
	E_2 (J/mol)	56,162	56,162	56,162	56,162
	m	1.48	1.48	1.48	1.48
	α_0	0.049	0.049	0.049	0.049
	Cure time (min)	59	90.7	60	112
	Overshoot (°C)	36	25	45	52
Conservative realisation	T_1 (°C)	144	136	177	157
	T_2 (°C)	186	206	–	177
	h (W/m^2/°C)	20.5	20.5	20.5	20.5
	E_2 (J/mol)	59,477	59,477	59,477	59,477
	m	1.1	1.1	1.1	1.1
	α_0	0.017	0.017	0.017	0.017
	Cure time (min)	73	97	76	118
	Overshoot (°C)	32	18	34	22
Standard deviation	Cure time (min)	2	1	2.6	1
	Overshoot (°C)	3.3	3.1	3.8	4.4

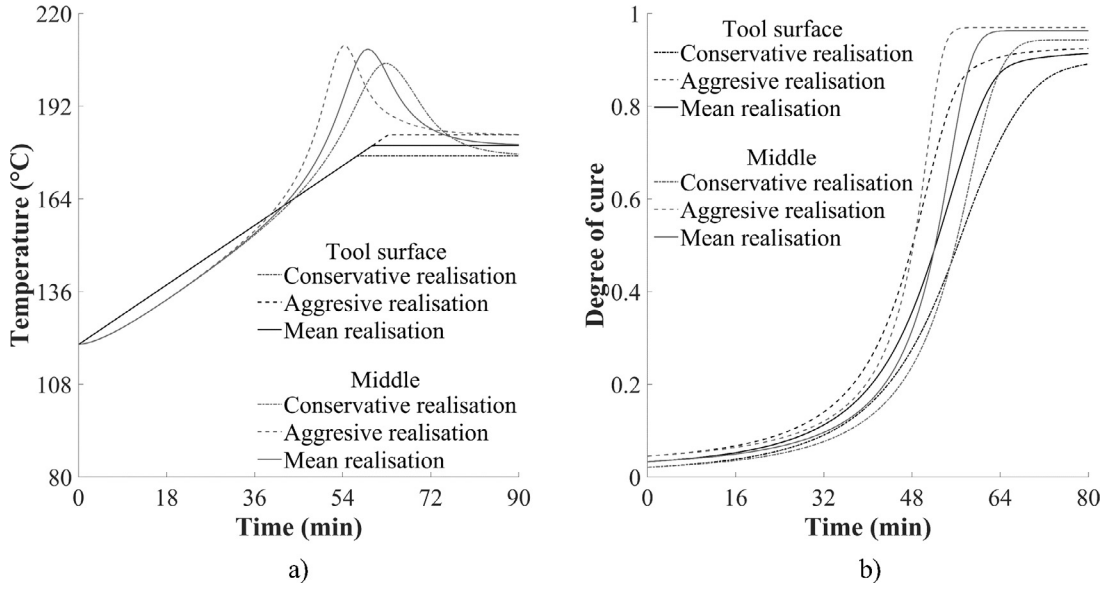

Fig. 11. One dwell standard profile: (a) temperature evolution; (b) degree of cure evolution.

design points and the results of the stochastic simulation for these points are reported in Table 6. The average cure time and temperature overshoot of deterministic and stochastic point are similar, whilst the cure time coefficient of variation is about 2.5% in both cases. The standard deviation of temperature overshoot of the point of deterministic optimisation is 6.6 °C, which is approximately twice that of the stochastic point. Furthermore, the nominal overshoot determined by deterministic simulation is lower by 7 °C compared to the average computed by stochastic simulation. Consequently, deterministic simulation provides a biased estimate of average overshoot underestimating risks. This explains the upward shifting of the stochastic Pareto front with respect to the deterministic points observed in Fig. 10. The temperature overshoot in the deterministic case is between 9 and 43 °C, whilst the stochastic one is in the range between 15 and 30 °C. The sensitivity of the deterministic point can be attributed to the higher first dwell temperature of its cure profile. These differences highlight the high sensitivity of deterministic optimal points and the robustness offered by stochastic optimal points.

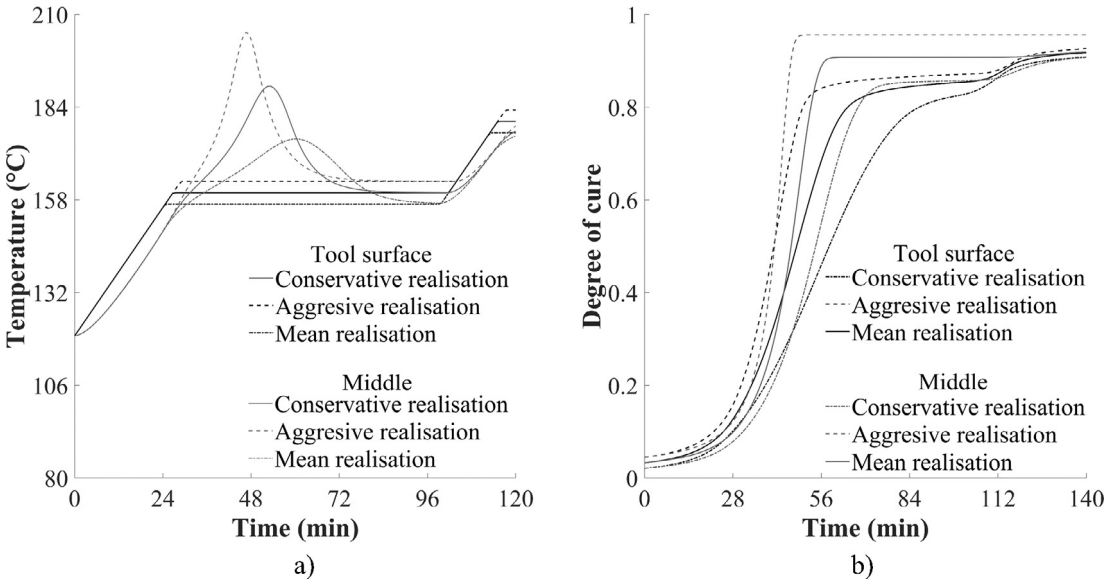

Fig. 12. Two dwell standard profile: (a) temperature evolution; (b) degree of cure evolution.

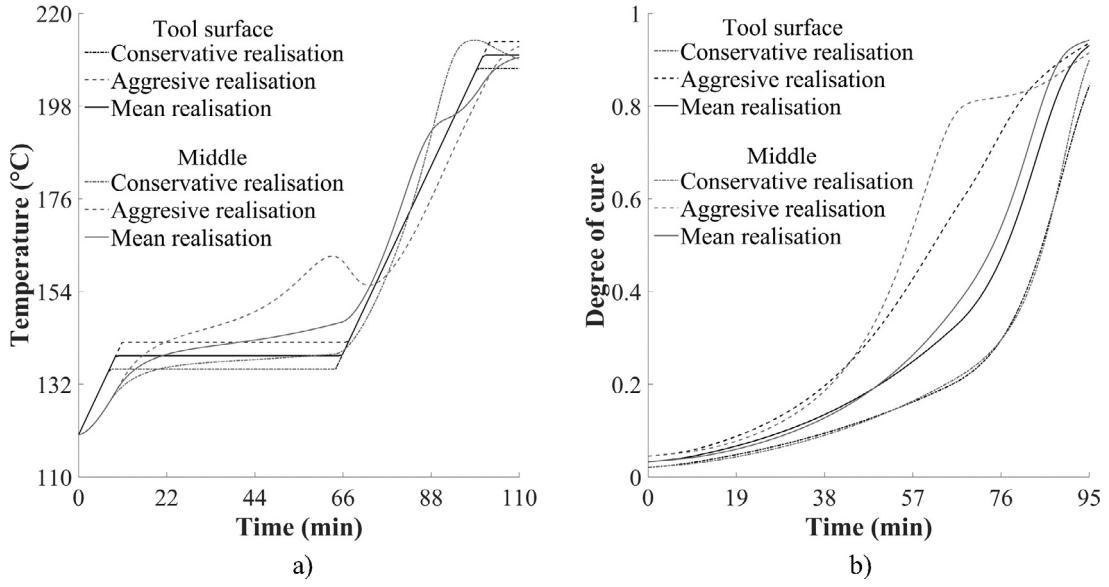

Fig. 13. Intermediate dwell optimal profile: (a) temperature evolution; (b) degree of cure evolution.

The stochastic Pareto front contains some points with cure time values twice as high as that of deterministic solutions. These points are located at the end of the horizontal region of the stochastic Pareto front and present low variations with standard deviations of 0.4 min and 2.5 °C for cure time and temperature overshoot respectively. These individuals are generated using conservative cure profiles with low first dwell temperature and long first dwell time. In these cases, overshoots are negligible and the cure process long. The vertical region of the stochastic Pareto front includes two points with temperature overshoot higher than 50 °C, a low cure time below 50 min and significant variations especially in the case of temperature overshoot with standard deviation between 4 and 4.5 °C. The cure time presents low variability with coefficient of variation of about 1.5%. The coefficient of variation of overshoot is 20%.

MC simulation of the two standard cure profiles of the resin system has been carried out. The first profile comprises two dwells at 160 °C and 180 °C [28] and the second one dwell at 180 °C [37]. A detailed analysis of the cure process has been carried out in order to uncover the qualitative characteristics of two optimal points with short and intermediate dwell profile and compare them with the standard cure profiles. Table 7 reports the inputs of this analysis. Figs. 11-14 illustrate the evolution of temperature and degree of cure at the tooling side and in the middle of the laminate for the three realisations. In the mean realisation stochastic variables (T_1, T_2, h, m, E_2, α_0) are equal to the mean values reported in Table 4. Aggressive and conservative realisations correspond to the cases where each stochastic variable was shifted by two standard deviations in the positive and negative direction according to the influence of each on cure time and overshoot. The aggressive realisation represents an extreme scenario in which all stochastic variables have values resulting in acceleration of the process, whilst the conservative realisation corresponds to values leading to a slower cure. The results obtained with the optimal points illustrate the significant improvements in terms of minimising both the mean value and the standard deviation of cure time and temperature overshoot in comparison with standard cure profiles and are reported in Table 7. In the intermediate dwell optimal profile, the average and the standard deviation of cure time were reduced by about 20% and 30% respectively compared to the standard two dwell profile. In addition, the

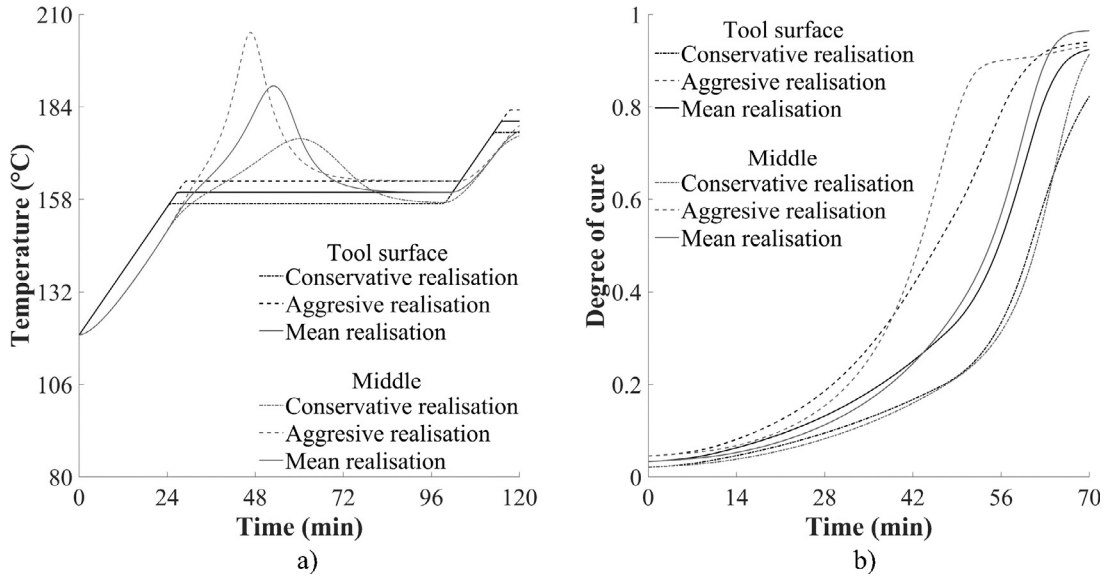

Fig. 14. Short dwell optimal profile: (a) temperature evolution; (b) degree of cure evolution.

optimal point presents a decrease of 60% in average temperature overshoot in comparison with both the one and two dwells standard profile. A higher first dwell temperature (Fig. 11a) results in an early reaction rate peak in the case of the one dwell standard profile. Consequently, the maximum temperature overshoot occurs during the first dwell. The selection of a one dwell profile with high dwell temperature results in low cure time and causes significant temperature overshoots that can reach up to about 50 °C in the aggressive realisation (Fig. 11a and 12a). The temperature evolution of the different realisations, as illustrated in Fig. 13a, highlights the stability of the intermediate optimal profile. The first dwell temperature is lower than that of the standard profiles reducing significantly exothermic effects and resulting in relative uniformity of temperature across the thickness. Also, the cure occurs almost at the same time in the three realisations, as shown in Fig. 13b, whereas for the standard profiles there are significant variations in cure duration between realisations (Fig. 11b and 12b). The short dwell optimal profile results in slightly faster cure time (Fig. 14b) than the standard one-dwell profile and approximately 40% reduction of cure time in comparison with the standard two dwell profile. The evolution of degree of cure through the thickness is more uniform for all realisations in the case of optimal profiles in comparison to standard profiles. This can be attributed to the fact that the cure reaction in the optimal solutions occurs more gradually than in the standard profiles, in which the high first dwell temperature accelerates aggressively the exothermic reaction. The average temperature overshoot of the short dwell optimal profile is lower by about 40%, whilst the standard deviation by about 20% and 10% compared to the standard one and two dwell profiles respectively.

Stochastic multi-objective optimisation yields a multi-dimensional Pareto front with optimal profiles that can be chosen based on the relative weightings of the different objectives relevant to specific applications. These are usually implied in the manufacturer's choices; e.g. in thick high cost components a low overshoot long cure process might be prioritised, whilst in inexpensive non-critical components a short and relatively unstable process might be preferred. In this sense, in an application in which duration is not prioritised cure cycles such as the intermediate dwell optimal case can be implemented with process duration of about 1.5 h and temperature overshoots in the range of 10–20 °C. In cases of high throughput lower specification composite parts, the short optimal profile can be chosen resulting in faster cure cycles of about 1 h, associated with temperature overshoots in the 20–35 °C range.

4. Conclusions

The stochastic multi-objective optimisation methodology developed in this study accounts for different sources of uncertainty by implementing a Monte Carlo simulation integrated into a GA to minimise temperature overshoot, cure time and their variability. Current deterministic optimisation methodologies generate optimal solutions that are sensitive to variations of the input parameters. The findings highlight the efficiency of stochastic optimisation in minimising cure time and temperature overshoot uncertainty in comparison with the standard cure profiles. The utilisation of surrogate modelling in a stochastic multi-objective optimisation problem makes the solution feasible in terms of computational time. The use of stochastic multi-objective optimisation can lead to considerably lower process durations reducing significantly manufacturing costs, whilst it can contribute to the development of more robust manufacturing processes in terms of outcome variability. The findings of the current study show that optimal cure profiles can be used to deliver faster processing and lower cost combined with improved quality while increasing robustness of the process outcome with respect to process uncertainty and materials variations.

Acknowledgments

This work was supported by the Engineering and Physical Sciences Research Council, through the grant 'Robustness performance optimisation for automated composites manufacture' (EP/K031430/1). Data underlying this study can be accessed through the Cranfield University repository at https://doi.org/10.17862/cranfield.rd.5706001.

References

[1] Skordos AA, Partridge IK. Inverse heat transfer for optimization and on-line thermal properties estimation in composites curing. Inv Probl Sci Eng 2004;12(2):157–72.
[2] Pillai V, Beris AN, Dhurjati P. Heuristics guided optimization of a batch autoclave curing process. Comput Chem Eng 1996;20(3):275–94.
[3] Rai N, Pitchumani R. Optimal cure cycles for the fabrication of thermosetting-matrix composites. Polym Compos 1997;18(4):566–81.
[4] Li M, Zhu Q, Geubelle PH, Tucker CL. Optimal curing for thermoset matrix composites. Thermochemical considerations. Polym Compos 2001;22(1):118–31.
[5] Yang ZL, Lee S. Optimised curing of thick section composite laminates. Mater Manuf Proc 2001;16(4):541–60.
[6] Carlone P, Palazzo GS. A simulation based metaheuristic optimization of the thermal cure cycle of carbon-epoxy composite laminates. In: Proceedings of The 14th international ESAFORM conference on material forming, Belfast, United Kingdom, April 27-29 2011. p.79–93.
[7] White SR, Hahn HT. Cure cycle optimization for the reduction of processing-induced

residual stresses in composite materials. J Compos Mater 1993;27(14):1352–78.
[8] Olivier P, Cottu JP. Optimisation of the co-curing of two different composites with the aim of minimising residual curing stress levels. Compos Sci Technol 1998;58(5):645–51.
[9] Bailleul JL, Sobotka V, Delaunay D, Jarny Y. Inverse algorithm for optimal processing of composite materials. Compos Part A Appl Sci Manuf 2003;34(8):695–708.
[10] Zhu Q, Geubelle PH. Dimensional accuracy of thermoset composites: shape optimization. J Compos Mater 2002;36(6):647–72.
[11] Khorsand AR, Raghavan J, Wang G. Tool-shape optimization to minimize warpage in autoclave processed L-shaped composite part. In: Proceedings of the 40th international SAMPE technical conference, Memphis, Tennessee, September 8–11 2008. p. 79–93.
[12] Gopal AK, Adali S, Verijenko VE. Optimal temperature profiles for minimum residual stress in the cure process of polymer composites. Compos Struct 2000;48(1):99–106.
[13] Ruiz E, Trochu F. Multi-criteria thermal optimization in liquid composite molding to reduce processing stresses and cycle time. Compos Part A Appl Sci Manuf 2006;37(6):913–24.
[14] Pantelelis NG. Optimised cure cycles for resin transfer moulding. Compos Sci Technol 2003;63(2):249–64.
[15] Struzziero G, Skordos AA. Multi-objective optimisation of the cure of thick components. Compos Part A Appl Sci Manuf 2017;93(2):126–36.
[16] Mesogitis TS, Skordos AA, Long AC. Uncertainty in the manufacturing of fibrous thermosetting composites: a review. Compos Part A Appl Sci Manuf 2014;57(2):67–75.
[17] Padmanabhan SK, Pitchumani R. Stochastic analysis of isothermal cure of resin systems. Polym Compos 1999;20(2):72–85.
[18] Mesogitis TS, Skordos AA, Long AC. Stochastic simulation of the influence of fibre path variability on the formation of residual stress and shape distortion. Polym Compos 2015;38(12):2642–52.
[19] Mesogitis TS, Skordos AA, Long AC. Stochastic simulation of the influence of cure kinetics uncertainty on composites cure. Compos Sci Technol 2015;110(4):145–51.
[20] Mesogitis TS, Skordos AA, Long AC. Stochastic heat transfer simulation of the cure of advanced composites. J Compos Mater 2016;50(21):2971–86.
[21] Acquah C, Datskov I, Mawardi A, Zhang F, Achenie LEK, Pitchumani R, et al. Optimization under uncertainty of a composite fabrication process using a deterministic one-stage approach. Comput Chem Eng 2006;30(5):947–60.
[22] Marc® volume B: Element library. <www.mscsoftware.com>; 2011.
[23] Marc® volume D: User subroutines and Special Routines. <www.mscsoftware.com>; 2011.
[24] Karkanas PI, Partridge IK. Cure modeling and monitoring of epoxy/amine resin systems. I. Cure kinetics modeling. J Appl Polym Sci 2000;77(7):1419–31.
[25] Pascault JP, Williams RJJ. Relationships between glass transition temperature and conversion. Polym Bull 1990;24(4):115–21.
[26] Farmer JD, Covert EE. Thermal conductivity of a thermosetting advanced composite during its cure. J Thermophys Heat Transf 1996;10(3):467–75.
[27] TohoTenax. Delivery programme and characteristics Tenax HTA filament yarn, Toho Tenax Europe GmbH, 2011.
[28] Hexcel® RTM 6 epoxy system for Resin Transfer Moulding monocomponent system product data. <www.hexcel.com>; 2009.
[29] Oliver MA, Webster R. A tutorial guide to geostatistics: computing and modelling variograms and kriging. Catena 2014;113(2):56–69.
[30] McKay MD, Beckman RJ, Conover WJ. A comparison of three methods for selecting values of input variables in the analysis of output from a computer code. Technometrics 1979;21(2):239–45.
[31] Skordos AA, Partridge IK. Cure kinetics modeling of epoxy resins using a non-parametric numerical procedure. Polym Eng Sci 2001;41(6):793–805.
[32] Sacks J, Welch WJ, Mitchell TJ, Wynn HP. Design and analysis of computer experiments. Stat Sci 1989;4(4):409–35.
[33] Santner T, Williams B, Notz W. The design and analysis of computer experiments. Springer Series in Statistics: Springer; 2003.
[34] Lophaven SN, Nielsen HB, Søndergaard J. DACE: a Matlab kriging toolbox. IMM, Informatics and Mathematical Modelling vol. 2. The Technical University of Denmark; 2002.
[35] RdF®. HFS-A, heat flux sensors. <www.rdfcorp.com>; 2018.
[36] Matsumoto M, Nishimura T. Mersenne Twister: a 623-dimensionally equidistributed uniform pseudo-random number generator. ACM Trans Model Comput Simul 1998;8(1):3–30.
[37] Hexcel® RTM 6 epoxy system for resin transfer moulding monocomponent system product data. <www.hexcel.com>; 2016.